

# Mapping molecular conformation and orientation of polyimide surfaces for homeotropic liquid crystal alignment by nonlinear optical spectroscopy

Masahito Oh-e\* and Hiroshi Yokoyama

*Yokoyama Nano-structured LC Project, ERATO, Japan Science & Technology Agency, 5-9-9 Tokodai, Tsukuba, Ibaraki-ken 300-2635, Japan*

Doseok Kim

*Department of Physics, Sogang University, Seoul 121-742, Korea*

(Received 29 December 2003; published 21 May 2004)

Surface-specific sum-frequency vibrational spectroscopy and second-harmonic generation were used to study the structures of polyimide (PI) surfaces for homeotropic liquid crystal (LC) alignment and the molecular orientation of LC adsorbates on these surfaces. The imide ring was perpendicular to the surface with one of CO bonds protruding out of the surface and the other pointing into the bulk rather than flat on the surface. The ester CO bond in the side chain was sticking out of the surface with a tilt angle of about  $45^\circ$ – $55^\circ$  from the surface normal, indicating that the rigid side chain core was, more or less, along the surface normal. The part of alkyl chain on the top of the side chain followed the orientation of the side chain core and protruded out of the surface with some gauche defects. The cyano biphenyl LC molecules were adsorbed on the PI preferentially with the terminal cyano group facing the PI surface.

DOI: 10.1103/PhysRevE.69.051705

PACS number(s): 61.30.Gd, 68.35.Bs, 78.66.Qn, 61.41.+e

## I. INTRODUCTION

Molecular alignment is of great practical importance for liquid crystal (LC) devices. Presently, LC alignment is most commonly achieved by mechanical rubbing of polymer-coated substrates [1,2]. The rubbed polyimide (PI) surface aligns an LC monolayer adsorbed on it via short-range interaction, which in turn aligns an LC bulk via LC molecular correlation [3–9]. This scheme however has some unwanted features in the manufacturing process and alternative methods capable of aligning LC films have been investigated. Among them, the nonrubbed technique with a specially designed PI is known to produce a homeotropic LC bulk alignment. This alignment is used for vertical alignment or multidomain vertical alignment LC modes [10] developed for wide viewing-angle LC displays. These LC modes have potential to compete with the other wide viewing-angle technique of the in-plane switching mode [11], in which a rubbed PI surface is used to yield a homogeneous LC bulk alignment. The conventional rubbed PI surfaces have been investigated by many different methods [12–18], but the nonrubbed surfaces for homeotropic alignment have not been studied carefully although the devices using homeotropic alignment is becoming more popular. It is well known that a hydrophobic surface of densely packed long alkyl chains generates a homeotropic LC alignment [2,19–21], however, the surface of PI commonly used nowadays for homeotropic alignment is not particularly hydrophobic, and detailed structural information of the surface is needed to understand the alignment mechanism.

Infrared-visible sum-frequency (SF) generation vibrational spectroscopy (SFVS) and second-harmonic generation (SHG) were used in our study since the techniques have been proven to be powerful surface analytical probes [22–25]. Being surface specific, they allow quantitative determination of molecular orientation and alignment at a polymer surface. The surface specificity arises because under the electric-dipole approximation, sum-frequency generation is forbidden in media with inversion symmetry, but allowed at a surface or interface where such symmetry is broken [26]. If the infrared input beam frequency is scanned over interfacial vibrational resonances, the sum-frequency signal from the interface is resonantly enhanced. This then yields a vibrational spectrum for the interface. The surface vibrational spectra with different input/output polarizations allow the determination of the orientation of selected atomic groups at the surface. Thus they provide information about surface structure and composition of a polymer. Applications of the techniques to rubbed surfaces of polyvinyl alcohol (PVA) [18] and some PIs [27–29] have shown that the surface polymer chains are well aligned along the rubbing direction [12–17], and so are the LC molecules adsorbed on them [3–9,30,31].

In this paper we report the results of our SFVS and SHG studies on the surfaces of PI known to yield homeotropic LC alignment, and the adsorbed LC monolayer. Our purpose is to find out how each molecular functional group of PI is oriented at the surface and how LC molecules sit on such a nonrubbed PI surface. The PI studied here has a side chain consisting of a rigid phenylbicyclohexane core connected to the main chain with an ester linkage and the topmost alkyl chain on the other side. For determination of molecular structure at the surface by SFVS, we focused on the imide CO, the ester CO that determines the rigid part of the side chain, and the alkyl chain at the end of the side chain. Then

\*Author to whom correspondence should be addressed. Electronic mail: oh-e@nanolc.jst.go.jp

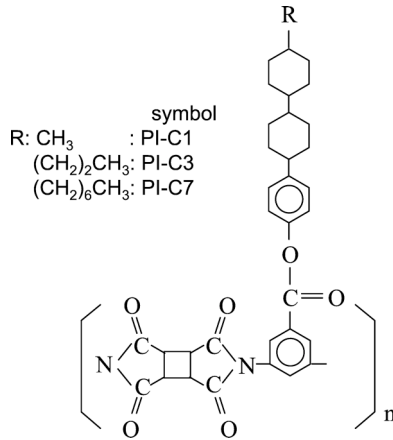


FIG. 1. Chemical structures of polyimides symbolized by PI-C1, PI-C3, and PI-C7, respectively.

we investigated the alignment of LC monolayer adsorbed on the above PI surface. SHG with different beam polarizations as well as SHG phase measurement was used to determine the polar orientation of LC molecules on the surface. Our results provided quantitative information on how the PI main chain and the side chain appear on a nonrubbed surface, and how the LC molecules sit on it.

## II. THEORETICAL BACKGROUND

The detailed theory of SFVS could be found elsewhere [22–25,32]. Here, for the convenience of later discussion, we give essential parts. SFVS from a medium is generated in reflection by the second-order nonlinear polarization  $P^{(2)}(\omega_{\text{SF}} = \omega_{\text{vis}} + \omega_{\text{ir}})$  induced by the incoming fields  $E_1(\omega_{\text{vis}})$  and  $E_2(\omega_{\text{ir}})$ . We assume here that the bulk contribution to SFVS is negligible, and the output intensity is given by

$$I(\omega_{\text{SF}}) = \frac{8\pi^3 \omega_{\text{SF}}^2 \sec^2 \beta_{\text{SF}}}{c^3} |\chi_{\text{eff}}^{(2)}|^2 |E_1(\omega_{\text{vis}})E_2(\omega_{\text{ir}})|^2, \quad (1)$$

where  $\beta_{\text{SF}}$  is the angle of the sum-frequency output with respect to the surface normal. The effective nonlinearity  $\chi_{\text{eff}}^{(2)}$  takes the form of

$$\chi_{\text{eff}}^{(2)} = [\hat{e}(\omega_{\text{SF}}) \cdot \vec{L}(\omega_{\text{SF}})] \cdot \vec{\chi}^{(2)} \cdot [\hat{e}(\omega_{\text{vis}}) \cdot \vec{L}(\omega_{\text{vis}})] \times [\hat{e}(\omega_{\text{ir}}) \cdot \vec{L}(\omega_{\text{ir}})], \quad (2)$$

with  $\hat{e}(\omega)$  being the unit polarization vector and  $\vec{L}(\omega)$  the tensorial Fresnel factor at frequency  $\omega$ . The nonlinear susceptibility  $\vec{\chi}^{(2)}$  is related to the molecular polarizability by

$$\vec{\chi}^{(2)} = \vec{\chi}_{\text{NR}}^{(2)} + N_s \int \vec{\alpha}^{(2)}(\Omega) f(\Omega) d\Omega, \quad (3)$$

where  $N_s$  is the surface density of an atomic group and  $f(\Omega)$  is an orientational distribution function. The resonant molecular hyperpolarizability  $\vec{\alpha}^{(2)}$  can be written as

$$\vec{\alpha}^{(2)}(\omega_{\text{ir}}, \Omega) = \sum_q \frac{\vec{\alpha}_q}{(\omega_{\text{ir}} - \omega_q) + i\Gamma_q}, \quad (4)$$

such that

$$\vec{\chi}^{(2)}(\omega_{\text{ir}}) = \vec{\chi}_{\text{NR}}^{(2)} + \sum_q \frac{\vec{A}_q}{(\omega_{\text{ir}} - \omega_q) + i\Gamma_q}, \quad (5)$$

with

$$\vec{A}_q = N_s \int \vec{\alpha}_q(\Omega) f(\Omega) d\Omega.$$

Here  $\chi_{\text{NR}}^{(2)}$  denotes the nonresonant contribution,  $\vec{\alpha}_q$ ,  $\omega_q$ , and  $\Gamma_q$  are the strength, resonant frequency, and damping constant of the  $q$ th resonant mode, respectively, and  $\Omega$  represents a set of orientational angles  $(\theta, \phi, \psi)$ . Scanning of  $\omega_{\text{ir}}$  over resonances yields a SFVS spectrum. Note that  $A_q$  and  $a_q$  are related by the same relation as  $\chi^{(2)}$  and  $\alpha^{(2)}$ . Analysis of SFVS with different polarization combinations using Eq. (3) allows us to deduce the quantitative information about the orientational distribution of atomic groups associated with vibrational modes on resonance.

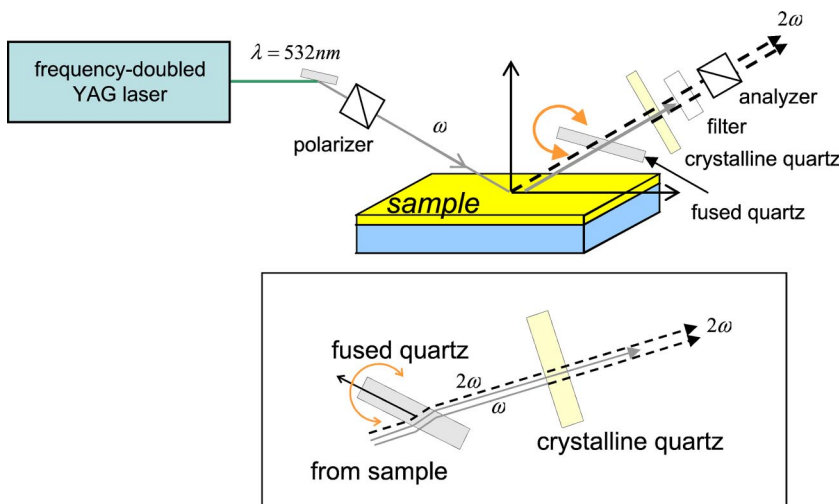


FIG. 2. (Color online) Schematic describing the experimental arrangement for SHG phase measurement.

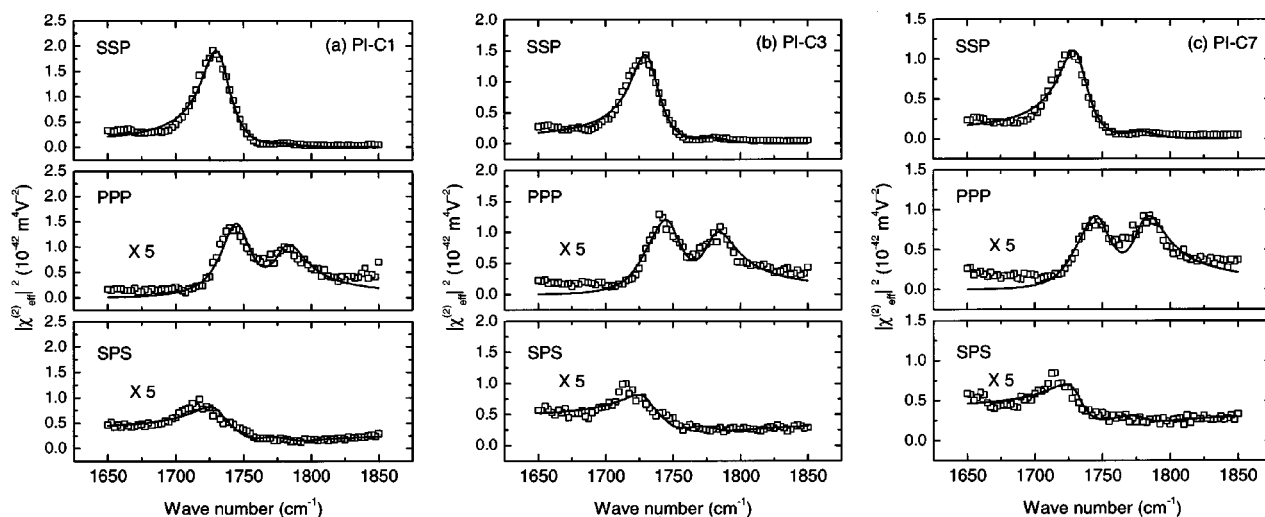


FIG. 3. SFVS spectra in the range of CO stretch with *ssp*, *ppp*, and *sps* polarization combinations for (a) PI-C1, (b) PI-C3, and (c) PI-C7. The spectra are normalized by the SF signal from a *z*-cut quartz.

The SFVS can be considered as a combined process of a resonant infrared excitation followed by an anti Stokes Raman process. The quantity  $a_q$  in Eq. (4) can be written in terms of the product of the infrared dipole derivative and the Raman polarizability tensor of the  $q$ th vibrational mode,  $\partial\mu/\partial Q_q$  and  $\partial\alpha^{(1)}/\partial Q_q$ , respectively,

$$(a_q)_{lmn} = -\frac{1}{2\omega_q} \frac{\partial \alpha_{lm}^{(1)}}{\partial Q_q} \frac{\partial \mu_n}{\partial Q_q}, \quad (6)$$

where  $Q_q$  denotes the normal mode coordinates, and the subindices  $(l, m, n)$  refer to the molecular coordinates  $(\xi, \eta, \zeta)$ .

### III. EXPERIMENT

The chemical structure of the PI samples studied are shown in Fig. 1. The film with a layer thickness of  $\sim 20$  nm was prepared by spin coating. To obtain uniform layers, the polyamic acid solution was filtered with a membrane filter. It was then dropped on a substrate to be spin-coated at 3000 rpm for 60 s. The samples were first prebaked at  $80^\circ\text{C}$  for 5 min for the evaporation of solvent and were then baked at  $250^\circ\text{C}$  for 20 min for imidization reaction. The LC (4'-*n*-pentyl-4-cyano-*p*-biphenyl, 5CB) monolayer on PI was prepared by thermal evaporation at  $60^\circ\text{C}$ , and SHG was measured *in situ* to monitor the deposition of LC. Formation

of a monolayer is indicated by the leveling of the SHG signal, because overlayer 5CB molecules on the surface are known to form quadrupolar pairs and contribute little to SHG.

For SFVS experiment, the main laser source was an EKSPLA Nd:YAG (YAG, yttrium aluminum garnet) laser ( $1.06\ \mu\text{m}$ , 30 mJ pulse energy, 25 ps pulse width, repetition rate 20 Hz). The tunable infrared beam was made with a AgGaS<sub>2</sub> crystal by difference frequency generation (DFG) using part of a  $1.06\ \mu\text{m}$  laser beam and tunable near-IR radiation from an optical parametric generator as inputs. This DFG stage generated tunable IR output of  $\sim 6\ \text{cm}^{-1}$  bandwidth in the  $3.3\text{--}3.6\ \mu\text{m}$  range with  $\sim 200\ \mu\text{J}$  pulse energy and in the  $5.4\text{--}6.1\ \mu\text{m}$  range with  $\sim 50\ \mu\text{J}$  pulse energy. The tunable IR beam was overlapped with a second-harmonic beam from the laser (532 nm) at the sample surface spatially and temporally with incidence angles of  $57^\circ$  and  $45^\circ$ , respectively. SF signal was recorded by averaging 200 shots per point at every  $2.5\ \text{cm}^{-1}$ .

The experimental arrangement for SHG phase measurement is shown in Fig. 2. We used a fused quartz of 1/8-in. thickness as a phase modulator and a thin *z*-cut crystalline quartz plate as reference SH generator in the reflected beam path [31,33]. The rotation of the fused quartz plate changed the relative phase between the fundamental field and the reflected SHG field from the sample, producing the interference fringe made from SH fields from the sample and the reference quartz crystal. By comparing the phase of the interference pattern from the sample with that from the other

TABLE I. Fitting parameters  $A_q$ ,  $\omega_q$ , and  $\Gamma_q$  of SFVS for the PI-C1 in the CO stretch region.

Mode	$\omega/\text{cm}^{-1}$	$\Gamma/\text{cm}^{-1}$	$A_{q,ssp}$	$A_{q,ppp}$	$A_{q,sps}$
Ester C=O ( <i>ester</i> , CO)	1732	13	$1.51 \pm 0.03$	$0.01 \pm 0.01$	$0.28 \pm 0.02$
Imide C=O ( <i>a-imide</i> , CO)	1745	14	$0.34 \pm 0.04$	$0.69 \pm 0.02$	$0.01 \pm 0.04$
Imide C=O ( <i>s-imide</i> , CO)	1780	15	$0.23 \pm 0.04$	$0.45 \pm 0.04$	$0.01 \pm 0.03$

LC layer of known polar orientation, the absolute orientation of the LC molecule could be deduced.

#### IV. RESULTS & ANALYSIS

##### A. Imide CO

Shown in Fig. 3 are the representative spectra of the PI's in the CO stretch vibrational region with three input/output polarization combinations: *ssp* (denoting *s*-polarized SF output, *s*-polarized visible input, and *p*-polarized infrared input, respectively), *sps*, and *ppp*. All the spectra can be fitted by Eq. (5) with three resonant modes at  $1732\text{ cm}^{-1}$ ,  $1745\text{ cm}^{-1}$ , and  $1780\text{ cm}^{-1}$ . They can be assigned, respectively, to the ester CO [ $q=\text{ester, CO}$ ] stretch of the side chain, the anti-symmetric ( $q=a\text{-imide, CO}$ ) and symmetric ( $q=s\text{-imide, CO}$ ) stretch vibrational modes for two coupled CO associated with each imide ring of the main chain [39]. The fitting results of the PI-C1 are in Table I. About the surface specificity of our measurement, the CO bonds not exposed to air are expected to form quadrupole pairs with CO bonds of neighboring molecular units, and would contribute very weakly to sum-frequency signal [35].

For the imide CO stretch, as seen in Fig. 4(a), these surface CO bonds lie in the imide core plane ( $\xi_1 - \eta_1$ ) and tilted by  $\sim 18^\circ$  from  $\eta_1$ . Their stretch vibrations are more strongly excited by IR field along  $\eta_1$  than  $\xi_1$ , and by symmetric Raman excitation in the  $\xi_1 - \eta_1$  plane. As for the ester CO stretch of the side chain, it is excited more easily by IR field along  $\xi_2$  direction as in Fig. 4(b). Inspection of the spectra in Fig. 3 already gives us qualitative information different from the PI that homogeneously aligns LCs in Ref. [29]. First, the *ssp* spectra of the imide ring are weaker than the *ppp* spectra, indicating that the inclination of the imide ring plane would be close to perpendicular to the surface rather than flat on the surface as was found for the PI for homogeneous LC alignment [27]. Second, the peak intensity of the ester CO stretch is very strong in *ssp* than the much smaller bump in the *sps* spectra, while the corresponding peak is hardly discernible in the *ppp* spectra. This suggests that a certain tilt angle of the ester CO bond from the surface normal would make the terms contributing to *ppp* signal to cancel each other and yield a negligibly small signal.

In the more quantitative analysis, we deduce the theoretical relationship between the tilt angle of CO bonds from the surface normal and the signal strength for *ssp*, *sps*, and *ppp* spectra. For an isotropic surface, the  $C_\infty$  symmetry allows three independent nonvanishing elements of  $(A_q)_{ijk}$  for non-resonant sum-frequency generation. They are [18]

$$(A_q)_{xxz} = (A_q)_{yyz},$$

$$(A_q)_{xzx} = (A_q)_{yzy} = (A_q)_{zxx} = (A_q)_{zyy}, \quad (A_q)_{zzz} \quad (7)$$

We can obtain the values of the nonvanishing  $(A_q)_{ijk}$  from the experimentally determined values of  $A_{q,\text{eff}}(P)$  for different input/output polarization combinations  $P$  using Eq. (2) as follows.

$$A_{q,\text{eff}}(ssp) = L_{yy}(\omega_{\text{SF}})L_{yy}(\omega_{\text{vis}})L_{zz}(\omega_{\text{ir}})\sin\beta_{\text{ir}}(A_q)_{yyz},$$

$$A_{q,\text{eff}}(sps) = L_{yy}(\omega_{\text{SF}})L_{zz}(\omega_{\text{vis}})L_{yy}(\omega_{\text{ir}})\sin\beta_{\text{vis}}(A_q)_{yzy},$$

$$A_{q,\text{eff}}(ppp)$$

$$\begin{aligned} &= -L_{xx}(\omega_{\text{SF}})L_{xx}(\omega_{\text{vis}})L_{zz}(\omega_{\text{ir}})\cos\beta_{\text{SF}}\cos\beta_{\text{vis}} \\ &\quad \times \sin\beta_{\text{ir}}(A_q)_{xxz} - L_{xx}(\omega_{\text{SF}})L_{zz}(\omega_{\text{vis}})L_{xx}(\omega_{\text{ir}})\cos\beta_{\text{SF}} \\ &\quad \times \sin\beta_{\text{vis}}\cos\beta_{\text{ir}}(A_q)_{xzx} + L_{zz}(\omega_{\text{SF}})L_{xx}(\omega_{\text{vis}})L_{xx}(\omega_{\text{ir}}) \\ &\quad \times \sin\beta_{\text{SF}}\cos\beta_{\text{vis}}\cos\beta_{\text{ir}}(A_q)_{zxx} \\ &\quad + L_{zz}(\omega_{\text{SF}})L_{zz}(\omega_{\text{vis}})L_{zz}(\omega_{\text{ir}}) \\ &\quad \times \sin\beta_{\text{SF}}\sin\beta_{\text{vis}}\sin\beta_{\text{ir}}(A_q)_{zzz}. \end{aligned} \quad (8)$$

Next we need to describe  $(A_q)_{ijk}$  in terms of molecular polarizability  $\vec{\alpha}_q$ . For this purpose, the first step is to find the nonvanishing elements of  $\vec{\alpha}_q$  in the molecular coordinates. As for the PI surface of previous study, the imide rings are expected to lie along the surface and only the CO bonds protruding out of the surface, namely, the upward pointing bonds contribute significantly to SFVS. Symmetry consideration then requires that the dominating elements of  $\vec{\alpha}_q$  are  $(a_q)_{\xi_1\xi_1\eta_1}$  and  $(a_q)_{\eta_1\eta_1\eta_1}$  for  $q=s\text{-imide, CO}$  and  $a\text{-imide, CO}$ . If we assume the main chains of our PI sample also run nearly parallel to the substrate, we have the following relations between tensorial elements of  $\vec{\alpha}_q$  in the lab coordinates and in the molecular coordinates for a PI molecular unit with orientation specified by  $\Omega = (\theta_1, \phi_1, \psi_1)$ .

$$\begin{aligned} (A_q)_{xxz} &= (A_q)_{yyz} = 2(a_q)_{\eta_1\eta_1\eta_1}\langle(\hat{\eta}_1 \cdot \hat{y})(\hat{\eta}_1 \cdot \hat{y})(\hat{\eta}_1 \cdot \hat{z})\rangle \\ &\quad + 2(a_q)_{\xi_1\xi_1\eta_1}\langle(\hat{\xi}_1 \cdot \hat{y})(\hat{\xi}_1 \cdot \hat{y})(\hat{\eta}_1 \cdot \hat{z})\rangle \\ &= 2(a_q)_{\eta_1\eta_1\eta_1}\langle\cos^2\phi_1\rangle\langle\sin^2\psi_1\cos\psi_1\rangle \\ &\quad + 2(a_q)_{\xi_1\xi_1\eta_1}\langle\sin^2\phi_1\rangle\langle\cos\psi_1\rangle \\ &= (a_q)_{\eta_1\eta_1\eta_1}\{\langle\cos\psi_1 - \cos^3\psi_1\rangle + r_{\text{co(imide)}}\langle\cos\psi_1\rangle\}, \\ (A_q)_{xzx} &= (A_q)_{yzy} = 2(a_q)_{\eta_1\eta_1\eta_1}\langle\cos^2\phi_1\rangle\langle\sin^2\psi_1\cos\psi_1\rangle \\ &= (a_q)_{\eta_1\eta_1\eta_1}\langle\cos\psi_1 - \cos^3\psi_1\rangle, \\ (A_q)_{zzz} &= 2(a_q)_{\eta_1\eta_1\eta_1}\langle\cos^3\psi_1\rangle, \end{aligned} \quad (9)$$

where  $r_{\text{co(imide)}} = (a_q)_{\xi_1\xi_1\eta_1}/(a_q)_{\eta_1\eta_1\eta_1}$  and we assumed  $\theta = 90^\circ$ . From Eqs. (8) and (9), we can calculate the theoretical curves of the expectable signal for each polarization combination. The parameters and Fresnel factors needed for the calculation is summarized in Table II. It should be reminded that the calculation would depend on the values of the interfacial refractive index  $n'_{\text{imide}}$  and  $r_{\text{co(imide)}}$ . To satisfy  $A_{q,\text{eff}}(ppp) > A_{q,\text{eff}}(ssp)$  and  $A_{q,\text{eff}}(sps) \approx 0$ ,  $\psi$  should be close to zero, indicating that the imide ring is oriented nearly perpendicular to the surface. So assuming a  $\delta$ -function distribution for  $\psi$ , we calculated the values of  $A_{q,\text{eff}}(ppp)/A_{q,\text{eff}}(ssp)$  as functions of  $n'_{\text{imide}}$  and  $r_{\text{co(imide)}}$ . Figure 5(a) shows contour plots for the calculated  $A_{q,\text{eff}}(ppp)/A_{q,\text{eff}}(ssp)$  as functions of  $n'_{\text{imide}}$  and  $r_{\text{co(imide)}}$ . There is ambiguity of the relationship between  $n'_{\text{imide}}$  and  $r_{\text{co(imide)}}$  even though the value of

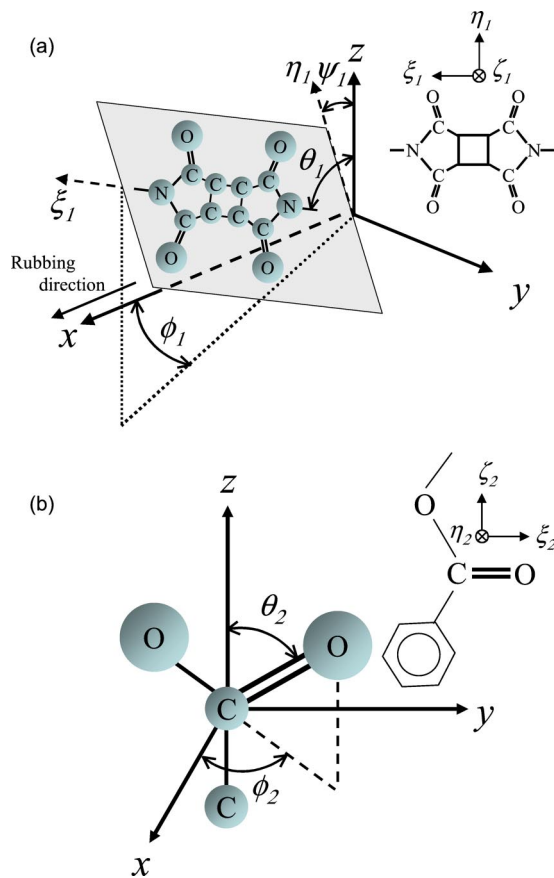


FIG. 4. (Color online) Coordinate systems defining the orientations of (a) an imide CO and (b) an ester CO.

$A_{q,\text{eff}}(ppp)/A_{q,\text{eff}}(ssp)$  is determined. However, if  $n'_{\text{imide}}$  is determined with a simple estimate of the local-field correction at the interface using the modified Lorentz model [36], we can then deduce the value of  $r_{\text{co(imide)}}$  with the value of  $A_{q,\text{eff}}(ppp)/A_{q,\text{eff}}(ssp)$ . Here we can assume  $n'_{\text{imide}} \approx 1.2$  with the modified Lorentz model. From the experimentally obtained values,  $A_{q,\text{eff}}(ppp)/A_{q,\text{eff}}(ssp) \approx 2.0$  for PI-C1, 1.5 for PI-C3, and 1.6 for PI-C7, by taking an average we deduced  $r_{\text{co(imide)}} \approx 0.47$  from Fig. 5(a). If the orientational distribution  $\sigma$  is assumed with a Gaussian form, the value of  $r_{\text{co(imide)}}$  becomes small accordingly as  $\sigma$  increases so as to keep  $A_{q,\text{eff}}(ppp)/A_{q,\text{eff}}(ssp)$  as indicated in Fig. 5(b). These con-

TABLE II. Parameters and Fresnel factors used for the calculation of the CO stretch region.  $n'$  ( $n'_{\text{imide}}$  or  $n'_{\text{ester}}$ ) is the air/PI interfacial refractive index for the imide or ester CO.

	$\omega_{\text{SF}}$	$\omega_{\text{vis}}$	$\omega_{\text{IR}}$
Wavelength $\lambda/\mu\text{m}$	0.487	0.532	5.73
Refractive index $n$	1.463	1.461	1.291
Beam angle $\beta/\text{deg}$	46.2	45.3	57.0
Fresnel factor $L_{xx}$	0.924	0.919	1.039
Fresnel factor $L_{yy}$	0.705	0.711	0.714
Fresnel factor $L_{zz}$	$1.076/n'^2$	$1.081/n'^2$	$0.961/n'^2$

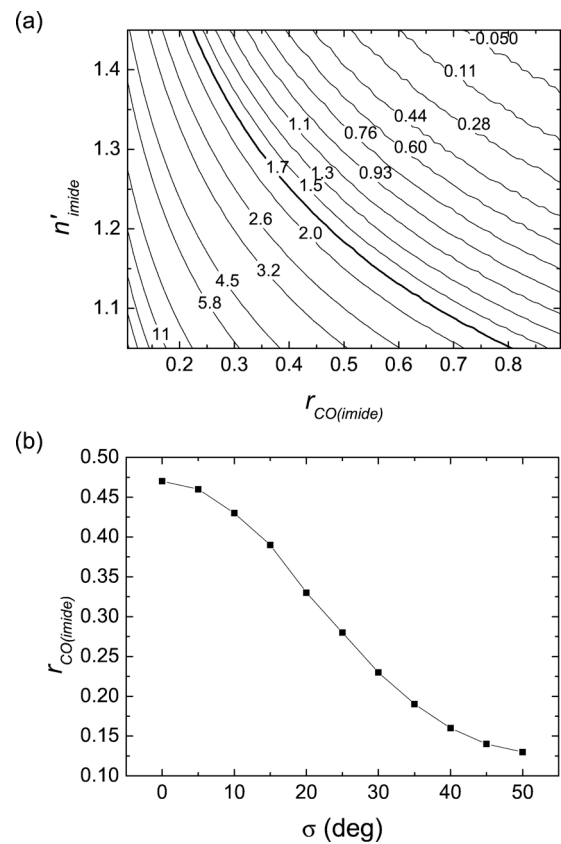


FIG. 5. (a) Contour lines for  $A_{s,\text{eff}}^{(2)}(ppp)/A_{s,\text{eff}}^{(2)}(ssp)$  as functions of  $n'_{\text{imide}}$  and  $r_{\text{CO(imide)}}$  with a  $\delta$  function. (b) Relationship of the values of  $r_{\text{CO(imide)}}$  to the orientational distribution  $\sigma$  for the constant value of  $A_{s,\text{eff}}^{(2)}(ppp)/A_{s,\text{eff}}^{(2)}(ssp)$ .

siderations allows us to have a picture that the imide ring is close to be perpendicular to the surface rather than flat on it.

## B. Ester CO

For the ester CO stretch that is cylindrically symmetric with the infrared transition moment along the symmetry axis  $\xi_2$ , there are only two nonvanishing independent elements in  $\vec{\alpha}_q$ ,  $(a_{\text{ester,co}})_{\eta_2\eta_2\xi_2} = (a_{\text{ester,co}})_{\xi_2\xi_2\xi_2}$  and  $(a_{\text{ester,co}})_{\xi_2\xi_2\xi_2}$ . The nonlinear susceptibilities  $(A_q)_{ijk}$  for an isotropic surface can then be described as

$$(A_{\text{ester,co}})_{xxz} = (A_{\text{ester,co}})_{yyz} = \frac{1}{2}\alpha_{\xi_2\xi_2\xi_2}[\langle\cos\theta_2\rangle(1+r_{\text{co(ester)})} - \langle\cos^3\theta_2\rangle(1-r_{\text{co(ester)})}]$$

$$(A_{\text{ester,co}})_{zxx} = (A_{\text{ester,co}})_{zyz} = (A_{\text{ester,co}})_{zxx} = (A_{\text{ester,co}})_{zyy} = \frac{1}{2}\alpha_{\xi_2\xi_2\xi_2}[\langle\cos\theta_2\rangle - \langle\cos^3\theta_2\rangle](1-r_{\text{co(ester)})}$$

$$(A_{\text{ester,co}})_{zzz} = \alpha_{\xi_2\xi_2\xi_2}[r_{\text{co(ester)}}\langle\cos\theta_2\rangle + \langle\cos^3\theta_2\rangle(1-r_{\text{co(ester)})}], \quad (10)$$

where  $r_{\text{co(ester)}} = (a_{\text{ester,co}})_{\eta_2\eta_2\xi_2}/(a_{\text{ester,co}})_{\xi_2\xi_2\xi_2}$ . The important feature that attention should be paid is that there appears almost no signal of the ester CO in the *ppp* spectra. From

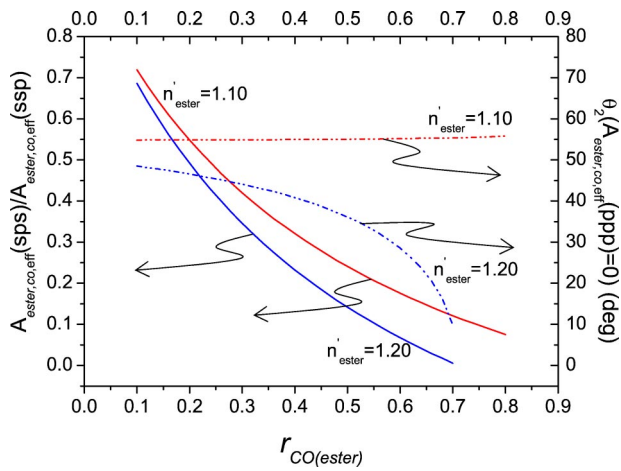


FIG. 6. (Color online)  $A_{\text{ester,co,eff}}^2(\text{sps})/A_{\text{ester,co,eff}}^2(\text{ssp})$  for the ester CO stretch at the tilt angle  $\theta_2$  where  $A_{\text{q,eff}}^2(\text{ppp}) \approx 0$  as functions of  $n'_{\text{ester}}$  and  $r_{\text{CO(ester)}}$  with a  $\delta$  function.

Eqs. (8) and (10), we can examine how the tilt angle  $\theta_2$  of the ester CO satisfies both  $A_{\text{ester,co,eff}}(\text{ppp}) \approx 0$  and the experimentally obtained values of  $A_{\text{ester,co,eff}}(\text{sps})/A_{\text{ester,co,eff}}(\text{ssp})$  at the same time. Again the exact values of  $r_{\text{co(ester)}}$  and  $n'_{\text{ester}}$  cannot be determined from our measurements, and we cannot have a unique value of  $\theta_2$ . The analysis, however, allows us to have a picture of the molecular unit conformation and orientation for the ester CO. Figure 6 shows the relationship of  $A_{\text{ester,co,eff}}(\text{sps})/A_{\text{ester,co,eff}}(\text{ssp})$  to  $r_{\text{co(ester)}}$  as a function of  $n'_{\text{ester}}$ . Here,  $A_{\text{ester,co,eff}}(\text{sps})/A_{\text{ester,co,eff}}(\text{ssp})$  is the value at the tilt angle  $\theta_2$  that satisfies  $A_{\text{ester,co,eff}}(\text{ppp}) \approx 0$ . For the analysis of the imide CO  $n'_{\text{imide}}$  was estimated to be 1.2, but  $n'_{\text{ester}}$  can be less than 1.2 because the ester CO is closer to air than the imide CO. So we put the two cases of  $n'_{\text{ester}} = 1.2$  and 1.1 in Fig. 6 assuming they are upper and lower bounds for the real  $n'_{\text{ester}}$  for the ester CO. From the experimentally obtained values,  $A_{\text{ester,co,eff}}(\text{sps})/A_{\text{ester,co,eff}}(\text{ssp}) \approx 0.19$  for PI-C1, 0.22 for PI

-C3, and 0.22 for PI-C7, we can then deduce from Fig. 6,  $r_{\text{co(ester)}} \approx 0.44$ ,  $\theta_2 \approx 40^\circ$  for  $n'_{\text{ester}} = 1.2$ , and  $r_{\text{co(ester)}} \approx 0.54$ ,  $\theta_2 \approx 55^\circ$  for  $n'_{\text{ester}} = 1.1$ . Unfortunately the ambiguity of  $n'_{\text{ester}}$  prevents us from deducing the exact value of  $\theta_2$  of the ester CO, however, the results do indicate that for all PIs the ester CO bonds are pointing outward from the surface. If the ester CO points inward, it would be buried into the bulk and form quadrupole pairs with other ester CO bonds of neighboring molecular units, resulting in the negligibly small signal. This is contradicting to our obtained spectra. Thus the ester CO is protruding out of the surface by the tilt angle of  $\theta_2 \approx 40^\circ - 55^\circ$  from the surface normal with the assumption of  $n'_{\text{ester}} = 1.1 - 1.2$ .

### C. Alkyl chain

To see the orientation of the alkyl chain on the top of the side chain core, we now present in Fig. 7 the SFVS spectra in the C-H stretch region of the PIs with three input/output polarization combinations. The spectra include six C-H vibrational stretches associated with the alkyl chains. The vibrational modes at approximately 2870, 2965, and 2953  $\text{cm}^{-1}$  can be assigned, respectively, to the symmetric ( $r^+$ ) and antisymmetric ( $r^-$ ) stretches of the terminal  $\text{CH}_3$  group of the alkyl chain and the Fermi resonance ( $r_{FR}^+$ ) between the symmetric  $\text{CH}_3$  stretch and its bending mode. The modes at 2843 and 2925  $\text{cm}^{-1}$  can be assigned to the symmetric ( $d^+$ ) and antisymmetric stretches of the  $\text{CH}_2$  groups on the chain, respectively. The peak at 2905  $\text{cm}^{-1}$  can be assigned to the C-H stretch of cyclohexane ring. The spectra for PIs with short and long chain lengths are different, mainly due to changes in chain conformation. All spectra can be fitted by the expression in Eq. (5) as described by the solid lines in Fig. 7. As a representative, the fitting parameters of the PI-C1 are summarized in Table III. The PI-C1 and PI-C3 have relatively shorter alkyl chains and their *ssp* spectra are dominated by the three peaks associated with  $\text{CH}_3$ , but two  $\text{CH}_2$  modes also show up. The latter must come from the  $\text{CH}_2$  groups on the cyclohexane link since their spectra are more or less

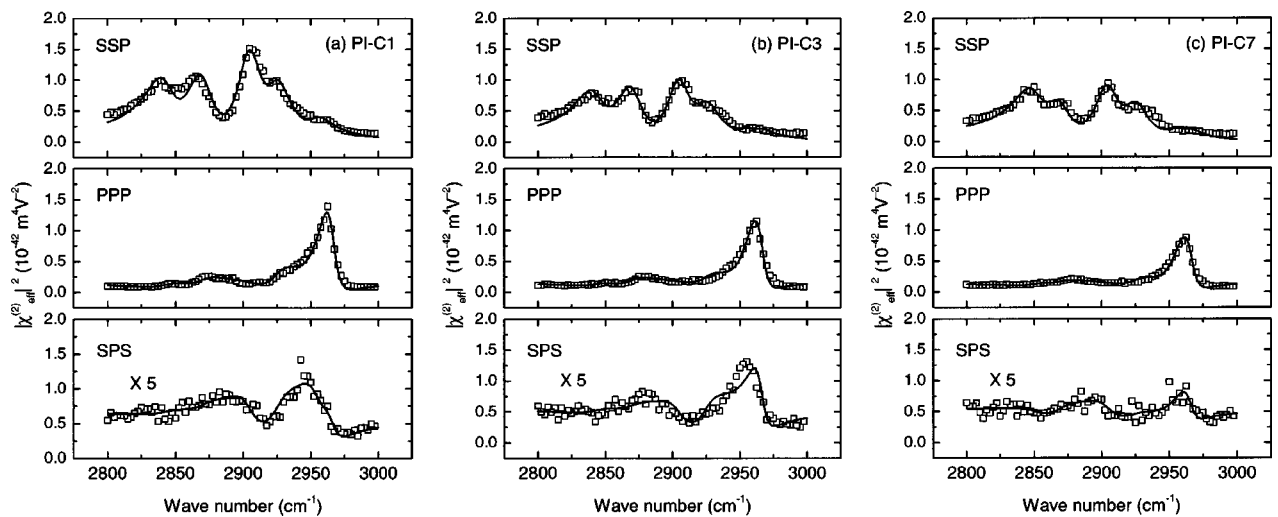


FIG. 7. SFVS spectra in the range of CH stretch with *ssp*, *ppp*, and *sps* polarization combinations for (a) PI-C1, (b) PI-C3, and (c) PI-C7. The spectra are normalized by the SF signal from a  $z$ -cut quartz.

similar to each other. The  $\text{CH}_3$  modes are prominent in the *ssp* spectra but not discernible in *sps*, indicating that  $\text{CH}_3$  would be oriented with its average along the surface normal. Compared to these spectra of PI-C1 and PI-C3, the spectra of PI-C7 exhibit some changes. The  $d^+$  mode for  $\text{CH}_2$  becomes more pronounced in the *ssp* spectrum while the  $r^+$  mode appears weaker than the  $d^+$  mode. These can be understood if we assume that the bicyclohexane rings of PI-C1, PI-C3, and PI-C7 are similarly oriented at the surfaces. The alkyl chain of PI-C3 forms all-trans and are oriented more or less along the surface normal, while a few gauche defects must set in for PI-C7 with the longer chain length to enhance the  $d^+$  mode in the *ssp* spectra.

The orientation of the terminal  $\text{CH}_3$  group can be determined by analyzing the  $r^+$  and/or  $r^-$  modes with the coordinates shown in Fig. 8[36]. For the  $\text{CH}_3$  group with a  $\text{C}_{3v}$  symmetry we can have the nonvanishing elements  $(A_{r^+})_{ijk}$  described by the molecular polarizabilities. There are only two nonvanishing independent elements in the molecular polarizability tensor,  $\tilde{\alpha}_q$ ,  $(a_{r^+})_{\xi_3\xi_3\xi_3}$  and  $(a_{r^+})_{\xi_3\xi_3\xi_3} = (a_{r^+})_{\eta_3\eta_3\xi_3} = r_{\text{CH}_3}(a_{r^+})_{\xi_3\xi_3\xi_3}$ . Here we take the symmetry axis as  $\xi_3$  for the  $r^+$  mode, and  $r_{\text{CH}_3}$  is the depolarization ratio. The four independent nonvanishing elements of the third-rank tensor  $A_q$  can be determined, together with the other parameters from fitting of the SFVS spectra obtained with different input/output polarization combinations. Since each  $(A_q)_{ijk}$  element is related to the molecular hyperpolarizability  $\tilde{\alpha}_q$ , we can find for an azimuthally isotropic surface the ratio of the effective  $(A_q)$  values for different polarization combinations. For the  $r^+$  mode, the nonvanishing elements  $(A_q)_{ijk}$  is given by

$$\begin{aligned} (A_{r^+})_{xxz} &= (A_{r^+})_{yyz} = \frac{1}{2}(a_{r^+})_{\xi_3\xi_3\xi_3}[\langle\cos\theta_3\rangle(1+r_{\text{CH}_3}) \\ &\quad - \langle\cos^3\theta_3\rangle(1-r_{\text{CH}_3})], \\ (A_{r^+})_{xzx} &= (A_{r^+})_{yzy} = (A_{r^+})_{zxx} = (A_{r^+})_{zyy} = \frac{1}{2}(a_{r^+})_{\xi_3\xi_3\xi_3}[\langle\cos\theta_3\rangle \\ &\quad - \langle\cos^3\theta_3\rangle](1-r_{\text{CH}_3}), \\ (A_{r^+})_{zzz} &= (a_{r^+})_{\xi_3\xi_3\xi_3}[r_{\text{CH}_3}\langle\cos\theta_3\rangle + \langle\cos^3\theta_3\rangle(1-r_{\text{CH}_3})]. \end{aligned} \quad (11)$$

For the  $r^-$  mode, we can deduce

$$\begin{aligned} (A_{r^-})_{xxz} &= (A_{r^-})_{yyz} = -(a_{r^-})_{\xi_3\xi_3\xi_3}(\langle\cos\theta_3\rangle - \langle\cos^3\theta_3\rangle), \\ (A_{r^-})_{xzx} &= (A_{r^-})_{yzy} = (A_{r^-})_{zxx} = (A_{r^-})_{zyy} = (a_{r^-})_{\xi_3\xi_3\xi_3}\langle\cos^3\theta_3\rangle, \\ (A_{r^-})_{zzz} &= 2(a_{r^-})_{\xi_3\xi_3\xi_3}(\langle\cos\theta_3\rangle - \langle\cos^3\theta_3\rangle). \end{aligned} \quad (12)$$

We can then deduce the orientational distribution of the  $\text{CH}_3$  group using the same analysis described in Ref. [36]. Here, however, we first analyze the ratio between  $(A_{r^-})_{yyz}$  and  $(A_{r^+})_{yyz}$ , and then use the ratio of the effective  $(A_{r^+})$  between the *ssp* and *ppp*. The latter is affected by the value of  $n'_{\text{CH}_3}$  while the former is not. So we can discuss and estimate the value of  $n'_{\text{CH}_3}$  for the  $\text{CH}_3$  group by making the two ways consistent. The ratio between  $(A_{r^-})_{yyz}$  and  $(A_{r^+})_{yyz}$  can simply

be deduced from Eqs. (11) and (12), and the ratio of the effective  $(A_{r^+})$  between the *ssp* and *ppp* is given by

$$\begin{aligned} \frac{A_{r^+,\text{eff}}^{(2)}(\text{ppp})}{A_{r^+,\text{eff}}^{(2)}(\text{ssp})} &= 0.0223 \frac{(\langle\cos\theta_3\rangle - \langle\cos^3\theta_3\rangle)(1-r_{\text{CH}_3})}{\langle\cos\theta_3\rangle(1+r_{\text{CH}_3}) - \langle\cos^3\theta_3\rangle(1-r_{\text{CH}_3})} \\ &\quad + \left(\frac{1.205}{n'^4}\right) \frac{2([r_{\text{CH}_3}\langle\cos\theta_3\rangle + \langle\cos^3\theta_3\rangle(1-r_{\text{CH}_3})]}{\langle\cos\theta_3\rangle(1+r_{\text{CH}_3}) - \langle\cos^3\theta_3\rangle(1-r_{\text{CH}_3})} \\ &\quad - 0.825, \end{aligned} \quad (13)$$

where we used the theoretical value of  $r_{\text{CH}_3}=2.2$  [37,38], and parameters and the Fresnel factors needed for the calculation are listed in Table IV. Figure 9(a) plots the relationship of  $(A_{r^-})_{yyz}/(A_{r^+})_{yyz}$  to the possible polar tilt angle  $\theta_3$  of the  $\text{CH}_3$  group using a  $\delta$  function and a Gaussian function with the distribution  $\sigma$ . From the experimentally obtained values,  $(A_{r^-})_{yyz}/(A_{r^+})_{yyz} \approx 0.009$  for PI-C1, 0.06 for PI-C3, and 0.10 for PI-C7, we can then deduce from Fig. 9(a),  $\theta_3 \approx 8^\circ$  with a  $\delta$  function for PI-C1,  $\theta_3 \approx 18^\circ$  with a  $\delta$  function and  $\theta_3 \approx 6^\circ$  with  $\sigma=10^\circ$  for PI-C3, and  $\theta_3 \approx 22^\circ$  with a  $\delta$  function,  $\theta_3 \approx 16^\circ$  with  $\sigma=10^\circ$  for PI-C7, respectively. The  $\text{CH}_3$  group is certainly pointing upward from the surface. Figure 9(b) shows the relationship of  $A_{r^+,\text{eff}}^{(2)}(\text{ppp})/A_{r^+,\text{eff}}^{(2)}(\text{ssp})$  to the possible polar tilt angle  $\theta_3$  of the  $\text{CH}_3$  group as a function of  $n'_{\text{CH}_3}$  assuming a  $\delta$  function. From the experimentally determined values,  $(A_{r^+})_{\text{ppp}}/(A_{r^+})_{\text{ssp}} \approx 0.23$  for PI-C1, 0.22 for PI-C3, and 0.17 for PI-C7,  $n'_{\text{CH}_3}$  must most likely be close to 1.0 to have the similar values of  $\theta_3$  obtained from the analysis of  $(A_{r^-})_{yyz}/(A_{r^+})_{yyz}$ . This is consistent with the fact that the  $\text{CH}_3$  group on the top of the side chain is the closest part to air. In Fig. 9(c), we demonstrates the relationship of  $A_{r^+,\text{eff}}^{(2)} \times (\text{ppp})/A_{r^+,\text{eff}}^{(2)}(\text{ssp})$  to the possible polar tilt angle  $\theta_3$  of the  $\text{CH}_3$  group using a  $\delta$  function and a Gaussian function with the distribution  $\sigma$  with the value of  $n'_{\text{CH}_3}=1.0$ .

#### D. LC orientation on PI surface

Since the PIs studied here is used for homeotropic LC alignment, we are interested in knowing how an LC molecule is oriented on those PIs and whether the LC molecule sits with the CN terminal facing the surface. We then studied the orientation of 5CB adsorbed on PI using SHG. The LC molecules were deposited on PI by thermal evaporation. During the evaporation, the *in situ* measurement showed that SHG increased monotonously and then leveled off [39]. The saturated signal from the 5CB layer was almost the same as in the case of other PIs for homogeneous LC alignment. This indicates that polar adsorption of 5CB on the PI surface for homeotropic LC alignment is probably achieved, leading to a coverage of the surface by polar-oriented 5CB molecules. Figure 10(a)–10(c) shows the SHG interference patterns from a 5CB monolayer on a fused quartz plate, a PI-C1 surface without and with a 5CB monolayer, respectively.

TABLE III. Fitting parameters  $A_q$ ,  $\omega_q$ , and  $\Gamma_q$  of SFVS for the PI-C1 in the C-H stretch region.

Mode	$\omega/\text{cm}^{-1}$	$\Gamma/\text{cm}^{-1}$	$A_{q,ssp}$	$A_{q,ppp}$	$A_{q,sps}$
$\text{CH}_2\text{-s}(d^+)$	2843	13	$0.74 \pm 0.02$	$-0.13 \pm 0.04$	$0.02 \pm 0.02$
$\text{CH}_3\text{-s}(r^+)$	2870	13	$0.95 \pm 0.02$	$-0.19 \pm 0.04$	$0.03 \pm 0.03$
$\text{CH}(m^+)$	2905	11	$1.08 \pm 0.01$	$0.05 \pm 0.04$	$-0.11 \pm 0.04$
$\text{CH}_2\text{-a}(d^-)$	2925	11	$0.63 \pm 0.02$	$-0.27 \pm 0.03$	$0.08 \pm 0.04$
$\text{CH}_3\text{-Fermi}(r_{FR}^+)$	2954	12	$0.30 \pm 0.03$	$-0.29 \pm 0.04$	$-0.17 \pm 0.03$
$\text{CH}_3\text{-as}(r^-)$	2966	7	$-0.01 \pm 0.03$	$0.67 \pm 0.01$	$-0.07 \pm 0.03$

5CB on quartz is known to lie with the CN terminal facing the surface [12,40]. The vector diagram of  $\chi^{(2)}$  in Fig. 10(d) shows that the polar-oriented 5CB molecules on PI-C1 must also have their CN terminals facing PI-C1; an opposite orientation of 5CB would change the sign of  $\chi_{5CB}^{(2)}$  and would lead to an SHG signal from 5CB/PI that decreases with increase of 5CB coverage, contrary to the observation.

For 5CB on PI-C1, we have  $\tilde{\chi}_{5CB/PI}^{(2)} \approx \tilde{\chi}_{PI}^{(2)} + \tilde{\chi}_{5CB}^{(2)}$ . To find  $\tilde{\chi}_{5CB}^{(2)}$  for the 5CB monolayer, we need to subtract  $\tilde{\chi}_{PI}^{(2)}$  from  $\tilde{\chi}_{5CB/PI}^{(2)}$ . Figure 10(d) shows a phase shift of  $57^\circ$  for  $\tilde{\chi}_{5CB/PI}^{(2)}$  relative to  $\tilde{\chi}_{PI}^{(2)}$ , and accordingly,  $\tilde{\chi}_{5CB}^{(2)}$  leads  $\tilde{\chi}_{PI}^{(2)}$  by  $75^\circ$ . Knowing the phase difference between  $\tilde{\chi}_{5CB/PI}^{(2)}$  and  $\tilde{\chi}_{PI}^{(2)}$ , we can find from

$$|\chi_{5CB}^{(2)}| = -|\chi_{PI}^{(2)}| \cos 75^\circ + \sqrt{|\chi_{5CB+PI}^{(2)}|^2 - |\chi_{PI}^{(2)}|^2 \sin^2 75^\circ}, \quad (14)$$

On the unrubbed PI-C3 surface, we have, for an isotropic azimuthal distribution,  $\chi_{zyy}^{(2)}/\chi_{zzz}^{(2)} = \langle \sin^2 \theta_3 \cos \theta_3 \rangle / \langle \cos^3 \theta_3 \rangle$ . [12] If we assume a  $\delta$  function for the LC molecular distribution in  $\theta_3$ , from  $\chi_{zyy}^{(2)}/\chi_{zzz}^{(2)} = 0.30$ , we then find that the 5CB molecule is tilted by  $\theta_3 \approx 38^\circ$  from the surface normal. For the 5CB on quartz, the tilt angle deduced in the same way with  $\chi_{zyy}^{(2)}/\chi_{zzz}^{(2)} = 0.44$  is  $\theta_3 \approx 43^\circ$ . For the 5CB on the PI for homogeneous alignment such as poly-*n*-hexyl-pyromellitic imide (P6) or polyoxydiphenylene-pyromellitic imide (PMDA-ODA), the tilt

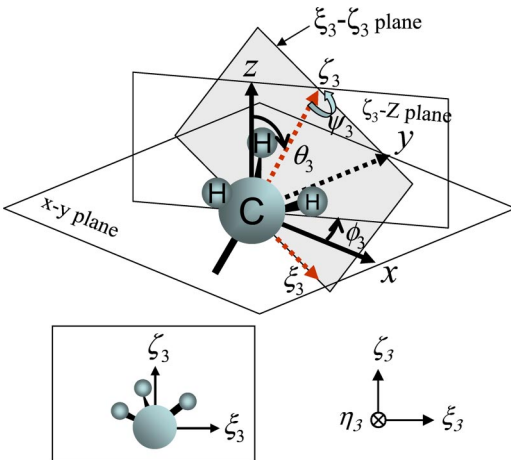


FIG. 8. (Color online) Coordinate systems defining the orientation of a  $\text{CH}_3$  group.

angle is  $\theta_3 \approx 60^\circ - 70^\circ$ . It is interesting to note that the 5CB molecule in the first monolayer on the PI-C3 is not completely oriented homeotropically and tilted to some extent from the surface normal although the angle is smaller than that on the PI for homogeneous alignment. The LC cell with a 5CB sandwiched by the PI-C3, however, did show the homeotropic LC bulk alignment. These results suggest that the homeotropic alignment with the PIs studied here is not determined by the orientation of the first LC monolayer.

## V. DISCUSSION

One of the interesting results is that the imide ring is almost perpendicular to the surface with one of the imide COs protruding out of the surface and the other pointing into the bulk. In the PI that homogeneously aligns LCs, the imide ring is, more or less, flat on the surface with a broad distribution, which is the case we studied before [27]. The orientation of the imide ring perpendicular to the surface would contribute to more dense packing of the molecular units than that flat on the surface. As a result, the side chain would pack densely at the surface as well and the distance to nearby side chains would become closer as the imide ring is perpendicular to the surface. The dense packing of the side chain due to the orientation of the imide ring perpendicular to the surface would be favorable condition for the dense packing of the side chain, hence the homeotropic LC alignment, in addition to a short molecular unit of the main chain per a side chain from the viewpoint of the chemical structure. Once the orientation of the ester CO is determined, the orientation of the rigid part of the phenylbicyclohexyl core in the side chain can be estimated. This is because the direction of the rigid

TABLE IV. Parameters and Fresnel factors used for the calculation of the  $\text{CH}_3$  stretch.  $n'_{\text{CH}_3}$  is the air/PI interfacial refractive index for the  $\text{CH}_3$  stretch.

	$\omega_{\text{SF}}$	$\omega_{\text{vis}}$	$\omega_{\text{IR}}$
Wavelength $\lambda/\mu\text{m}$	0.461	0.532	3.48
Refractive index $n$	1.465	1.461	1.410
Beam angle $\beta/\text{deg}$	46.7	45.3	57.0
Fresnel factor $L_{xx}$	0.927	0.919	1.023
Fresnel factor $L_{yy}$	0.701	0.711	0.749
Fresnel factor $L_{zz}$	$1.073/n_{\text{CH}_3}^{\prime 2}$	$1.081/n_{\text{CH}_3}^{\prime 2}$	$0.977/n_{\text{CH}_3}^{\prime 2}$

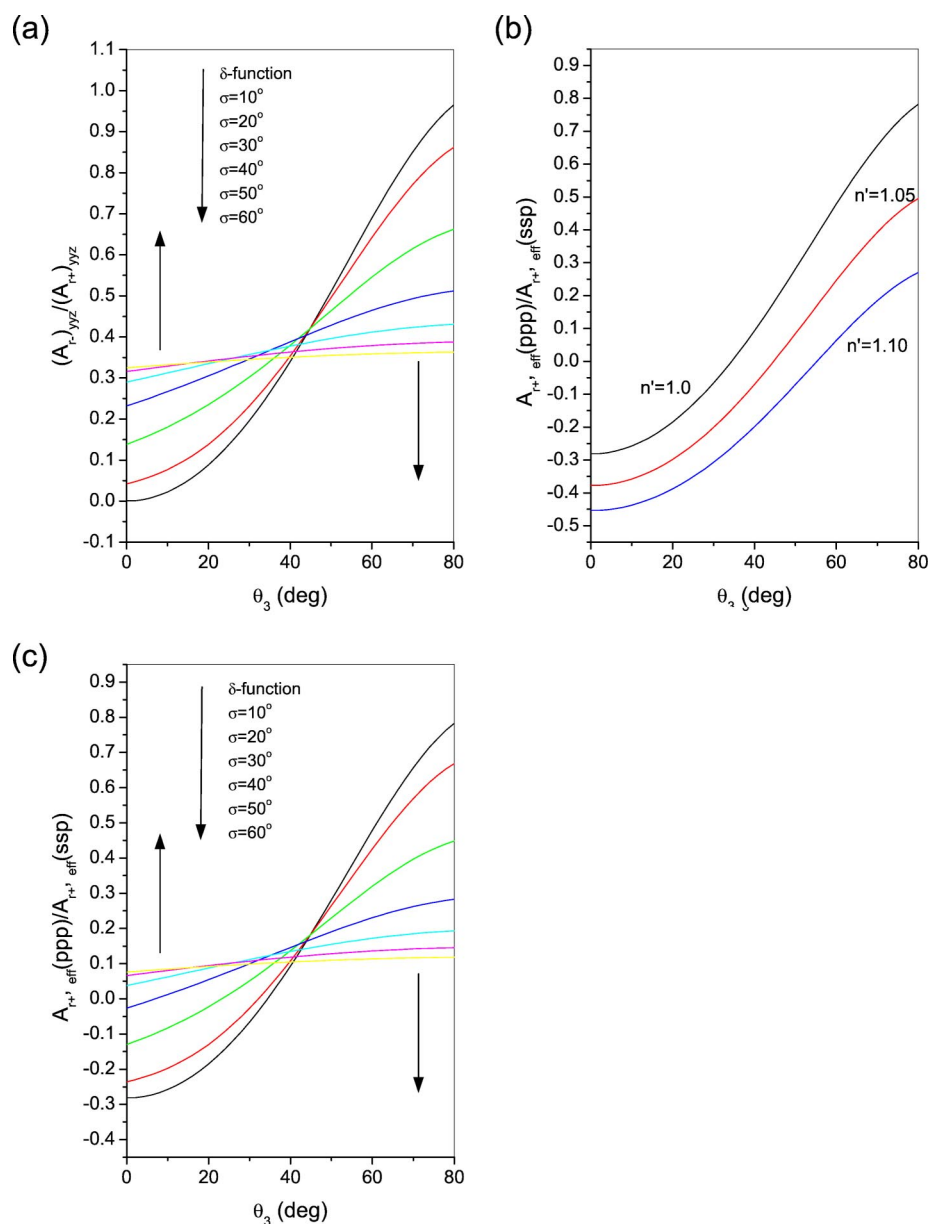


FIG. 9. (Color online) (a)  $(A_{r^+}^{(2)})_{yyz}/(A_{r^+})_{yyz}$  vs  $\theta_3$  of the  $\text{CH}_3$  group with a  $\delta$  function and a Gaussian function. (b)  $A_{r^+,eff}^{(2)} \times (ppp)/A_{r^+,eff}^{(2)}(ssp)$  vs  $\theta_3$  as a function of  $n'_{\text{CH}_3}$  with a  $\delta$  function. (c)  $A_{r^+,eff}^{(2)}(ppp)/A_{r^+,eff}^{(2)}(ssp)$  vs  $\theta_3$  of the  $\text{CH}_3$  group with a  $\delta$  function and a Gaussian function assuming  $n'_{\text{CH}_3} = 1.0$ .

part of the side chain that connected to the oxygen atom of the ester group is determined by the orientation of the ester  $\text{C}=\text{O}$  bond and the corresponding molecular conformational considerations as shown in Fig. 11. If the ester  $\text{CO}$  is oriented by  $40^\circ$ – $55^\circ$  from the surface normal, the phenyl to oxygen bond of the rigid part is more or less along the surface normal by within about  $10^\circ$  assuming that the plane of the phenylene ring in the side chain is the same as that of the ester group to form a  $\pi$  electron conjugated system among the phenylene ring, the ester  $\text{C}=\text{O}$  bond and the lone pair of the oxygen atom. The two cyclohexane rings are chair-shaped conformation and connected to each other by trans configuration since the material was synthesized in such a way. It is well known that the long alkyl chains densely formed at the surface such as octadecyltrichlorosilane (OTS) and *n*-dimethyl-*n*-octadecyl-3-aminopropyl-trimethoxysilyl chloride (DMOAP) surfactant monolayers give a hydrophobic surface and a homeotropic LC alignment with the alkyl chain facing the surface due to the low surface energy and

the chain-chain interaction [2,19–21]. On such a surface, the first monolayer determines the homeotropic bulk alignment. Interestingly, this is not the case for the PIs for the homeotropic LC alignment studied here since an LC molecule sits on the PI with the CN terminal facing the surface, indicating that the surface is not so hydrophobic. Furthermore, the LC molecules in the first monolayer on the PI surface are not completely along the surface normal but tilted by about  $38^\circ$ , although the angle is smaller than that obtained on the PI for homogeneous LC alignment. The tilt angle of the LC monolayer may be induced by the rigid part of the side chain. The fact that the LC monolayer is tilted from the surface normal with the CN facing the surface is not the case for the conventional hydrophobic homeotropic alignment. As long as the first LC monolayer at the air/PI interface is concerned, we have found that there seems no big difference between the PIs for homogenous and homeotropic LC alignments. An LC film sandwiched by the PI, however, does give a homeotropic LC bulk alignment, suggesting that the mechanism of

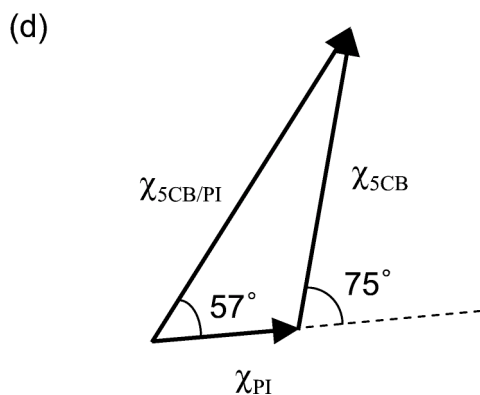
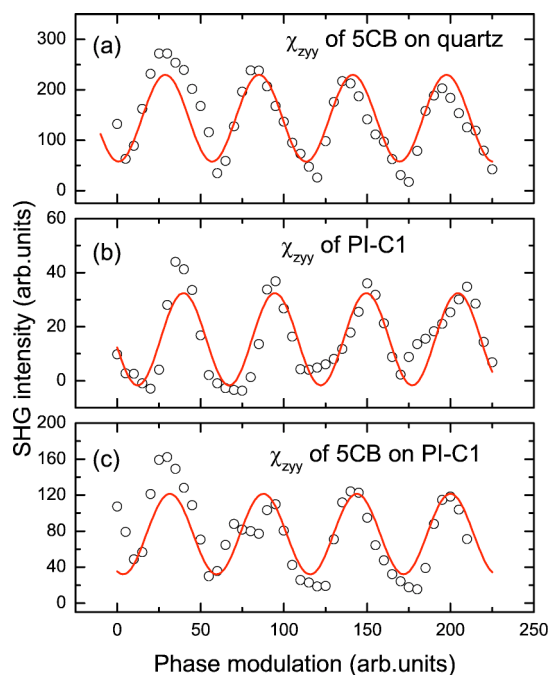


FIG. 10. Experimental data and line fits for SHG phase measurements of (a) a 5CB monolayer on quartz, and the PI-C3 (b) without and (c) with a 5CB monolayer. (d) Schematic phase relationship of  $\chi^{(2)}$  for a 5CB monolayer on a PI surface.  $\chi_{PI}^{(2)}$ ,  $\chi_{5CB}^{(2)}$ , and  $\chi_{5CB/PI}^{(2)}$  are the susceptibilities of the PI surface, the 5CB monolayer, and the 5CB monolayer on the PI, respectively.

the homeotropic alignment is possibly different from the conventional hydrophobic surface and the alignment in this case would be determined by properties of both the surface and the bulk.

## VI. CONCLUSION

In conclusion, we have shown that the SFVS and SHG can be used to quantitatively determine the average orienta-

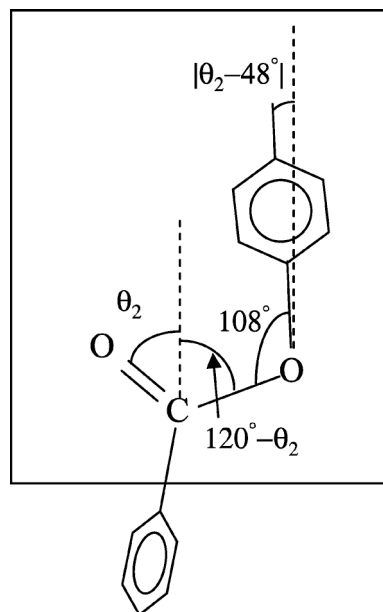


FIG. 11. Schematic describing the molecular conformation of the ester CO group in the side chain.

tion and conformation of selective functional groups and segments of surface structures. As a demonstrating system, the PIs for homeotropic LC alignment has been studied to understand the molecular conformation and orientation at the surface and the interaction of the LC molecules on it. The orientation of the imide CO located in the main chain, the ester CO in the side chain, and the alkyl chain on the top of the side chain can be determined if the appropriate refractive indices for the interface are fixed. The LC molecule sit on the PI surface with the terminal CN facing the surface, which is not the case for the conventional hydrophobic homeotropic alignment.

## ACKNOWLEDGMENTS

We would like to thank Shizuo Murata and Dr. Yikio Hirano of Chisso Petrochemical Corporation for providing us the polyimides used in this study and for pretilt angle measurements, respectively. We would also like to acknowledge the useful advice from Professor Y. R. Shen in University of California at Berkeley. M. O. gratefully acknowledges Hitachi Displays, Ltd. for financial support. D. K. was supported by the Sogang University Special Research Grant in 2001.

- [1] C. Mauguin, *Bull. Soc. Fr. Mineral.* **34**, 71 (1911).
- [2] J. Cognard, *Mol. Cryst. Liq. Cryst.* **51**, 1 (1982).
- [3] J. M. Geary, J. W. Goodby, A. R. Kmetz, and J. S. Patel, *J. Appl. Phys.* **62**, 4100 (1987).
- [4] N. A. J. M. van Aerle, M. Barmento, and R. W. Hollenng, *J. Appl. Phys.* **74**, 3111 (1993).
- [5] X. Zhuang, L. Marrucci, and Y. R. Shen, *Phys. Rev. Lett.* **73**, 1513 (1994).
- [6] K. Sawa, K. Sumiyoshi, Y. Hirai, K. Tateishi, and T. Kamejima, *Jpn. J. Appl. Phys., Part 1* **33**, 6273 (1994).
- [7] Y. Ouchi, I. Mori, M. Sei, E. Ito, T. Araki, H. Ishii, K. Seki, and K. Kondo, *Physica B* **208/209**, 407 (1995).
- [8] M. F. Toney, T. P. Russell, J. A. Logan, H. Kikuchi, J. M. Sands, and S. K. Kumar, *Nature (London)* **374**, 709 (1995).
- [9] I. Hirotsawa, *Jpn. J. Appl. Phys., Part 1* **35**, 5873 (1996).
- [10] Y. Koike, S. Kataoka, T. Sasaki, H. Chida, H. Tsuda, A. Takeda, K. Ohmuro, T. Sasabayashi, and K. Okamoto, in *Proceedings of the 4th International Display Workshop*, edited by IDW'97 Committee (Society for Information Display, Nagoya, 1997), p. 159.
- [11] M. Oh-e and K. Kondo, *Appl. Phys. Lett.* **67**, 3895 (1995); M. Oh-e and K. Kondo, *Liq. Cryst.* **22**, 379 (1997).
- [12] W. Chen, M. B. Feller, and Y. R. Shen, *Phys. Rev. Lett.* **63**, 2665 (1989); M. B. Feller, W. Chen, and Y. R. Shen, *Phys. Rev. A* **43**, 6778 (1991).
- [13] M. Barmentlo, R. W. J. Hollering, and N. A. J. M. van Aerle, *Phys. Rev. A* **46**, R4490 (1992); X. Zhuang, L. Marrucci, and Y. R. Shen, *Phys. Rev. Lett.* **73**, 1513 (1994).
- [14] D. Johannsmann, H. Zhou, P. Sonderkaer, H. Wierenga, B. O. Myrvold, and Y. R. Shen, *Phys. Rev. E* **48**, 1889 (1993).
- [15] K. Shirota, M. Yaginuma, T. Sakai, K. Ishikawa, H. Takezoe, and A. Fukuda, *Appl. Phys. Lett.* **69**, 164 (1996); T. Sakai, J. Yoo, Y. Kinoshita, K. Ishikawa, H. Takezoe, A. Fukuda, T. Nihira, and H. Endo, *ibid.* **71**, 2274 (1997).
- [16] M. G. Samant, J. Stöhr, H. R. Brown, T. P. Russell, J. M. Sands, and S. K. Kumar, *Macromolecules* **29**, 8334 (1996); K. Weiss, C. Wöll, E. Böhm, B. Fiebranz, G. Forstmann, B. Peng, V. Scheumann, and D. Johannsmann, *ibid.* **31**, 1930 (1998); J. Stöhr, M. G. Samant, A. Cossy-Favre, J. Diaz, Y. Momoi, S. Odahara, and T. Nagata, *ibid.* **31**, 1942 (1998); A. Cossy-Favre, J. Diaz, Y. Liu, H. R. Brown, M. G. Samant, J. Stöhr, A. J. Hanna, S. Anders, and T. P. Russell, *ibid.* **31**, 4957 (1998).
- [17] K.-W. Lee, A. Lien, J. H. Stathis, and S.-H. Paek, *Jpn. J. Appl. Phys., Part 1* **36**, 3591 (1997); S.-H. Paek, C. J. Durning, K.-W. Lee, and A. Lien, *J. Appl. Phys.* **83**, 1270 (1998).
- [18] X. Wei, X. Zhuang, S.-C. Hong, T. Goto, and Y. R. Shen, *Phys. Rev. Lett.* **82**, 4256 (1999); X. Wei, S.-C. Hong, X. Zhuang, T. Goto, and Y. R. Shen, *Phys. Rev. E* **62**, 5160 (2000).
- [19] F. J. Kahn, *Appl. Phys. Lett.* **22**, 386 (1973).
- [20] H. Hsiung, Th. Rasing, and Y. R. Shen, *Phys. Rev. Lett.* **57**, 3065 (1986); W. Chen, L. J. Martinez-Miranda, H. Hsiung, and Y. R. Shen, *ibid.* **62**, 1860 (1989).
- [21] B. Alkhairalla, H. Allinson, N. Boden, S. D. Evans, and J. R. Henderson, *Phys. Rev. E* **59**, 3033 (1999).
- [22] X. D. Zhu, H. Suhr, and Y. R. Shen, *Phys. Rev. B* **35**, 3047 (1987).
- [23] Y. R. Shen, *Annu. Rev. Phys. Chem.* **40**, 327 (1989).
- [24] Y. R. Shen, in *Frontier in Laser Spectroscopy*, Proceedings of the International School of Physics "Enrico Fermi," Course CXX, edited by T. W. Hansch and M. Inguscio (North Holland, Amsterdam, 1994), p. 139.
- [25] Y. R. Shen, *Surf. Sci.* **299/300**, 551 (1994).
- [26] Y. R. Shen, *The Principle of Nonlinear Optics* (Wiley, New York, 1984).
- [27] D. Kim, M. Oh-e, and Y. R. Shen, *Macromolecules* **34**, 9125 (2001).
- [28] M. Oh-e, A. I. Lvovsky, X. Wei, and Y. R. Shen, *J. Chem. Phys.* **113**, 8827 (2000).
- [29] M. Oh-e, D. Kim, and Y. R. Shen, *J. Chem. Phys.* **115**, 5582 (2001).
- [30] M. Oh-e, S.-C. Hong, and Y. R. Shen, *J. Phys. Chem. B* **104**, 7455 (2000).
- [31] S.-C. Hong, M. Oh-e, X. Zhuang, and Y. R. Shen, *Phys. Rev. E* **63**, 051706 (2001).
- [32] Y. R. Shen, in *Nonlinear Spectroscopy for Molecular Structure Determination*, edited by R. W. Field, E. Hirota, J. P. Maier, and S. Tsuchiya, IUPAC Commission on Molecular Structure and Spectroscopy (Blackwell Science, UK, Oxford, 1998), Chap. 10.
- [33] J. Y. Huang and A. Lewis, *Biophys. J.* **55**, 835 (1989).
- [34] H. Ishida, S. T. Wellinghoff, E. Baer, and J. L. Koenig, *Macromolecules* **13**, 826 (1980).
- [35] X. Wei, S.-C. Hong, A. I. Lvovsky, H. Held, and Y. R. Shen, *J. Phys. Chem. B* **104**, 3349 (2000).
- [36] X. Zhuang, P. B. Miranda, D. Kim, and Y. R. Shen, *Phys. Rev. B* **59**, 12632 (1999).
- [37] K. M. Gough, *J. Phys. Chem.* **91**, 2424 (1989).
- [38] D. Zhang, J. H. Gustow, T. F. Heinz, K. B. Eisenthal, *J. Phys. Chem.* **98**, 13729 (1994).
- [39] C. S. Mullin, P. Guyot-Sionnest, and Y. R. Shen, *Phys. Rev. A* **39**, 3745 (1989).
- [40] P. Guyot-Sionnest, H. Hsiung, and Y. R. Shen, *Phys. Rev. Lett.* **57**, 2963 (1986).